# Validation of ozone monitoring instrument $SO_2$ measurements in the Okmok volcanic cloud over Pullman, WA, July 2008

Elena Spinei,[1] Simon A. Carn,[2] Nickolay A. Krotkov,[3] George H. Mount,[1] Kai Yang,[3] and Arlin Krueger[4]

Received 16 November 2009; revised 15 April 2010; accepted 3 May 2010; published 18 September 2010.

[1] The ozone monitoring instrument (OMI), launched on the EOS/Aura satellite in July 2004, makes daily global observations of natural and anthropogenic $SO_2$ emissions with unprecedented spatial resolution. Here we present the first robust comparison of OMI volcanic $SO_2$ retrievals with ground−based instrumentation, using direct Sun observations of the Okmok volcanic cloud from Washington State University (WSU) in Pullman, WA on 18–20 July 2008. These measurements were made by the multifunction differential optical absorption spectroscopy (MFDOAS) instrument developed at WSU, as the Okmok cloud drifted over Pullman in the upper troposphere and lower stratosphere (UTLS). Observation conditions were favorable with cloud-free skies and a relatively homogeneous volcanic cloud distribution on OMI ground pixel scales (~20–50 km). Movement of the Okmok cloud north and south of Pullman over a period of several days permitted comparison with three OMI overpasses with $SO_2$ column amounts above the $SO_2$ background level. The total $SO_2$ columns measured by MFDOAS during OMI overpasses were 3.11 ± 0.23 Dobson units (DU), 1.75 ± 0.16 DU and 1.22 ± 0.18 DU (1 DU = $2.69 \times 10^{16}$ molecules/cm$^2$ = 0.029 g/m$^2$). Comparison of ground-based direct Sun and operational and off-line OMI retrievals show an excellent agreement, providing the first validation of OMI measurements of volcanic $SO_2$ in the UTLS.

**Citation:** Spinei, E., S. A. Carn, N. A. Krotkov, G. H. Mount, K. Yang, and A. Krueger (2010), Validation of ozone monitoring instrument $SO_2$ measurements in the Okmok volcanic cloud over Pullman, WA, July 2008, *J. Geophys. Res.*, *115*, D00L08, doi:10.1029/2009JD013492.

## 1. Introduction

[2] Sulfur dioxide ($SO_2$) is a trace gas regulated by the U. S. Environmental Protection Agency (EPA) that negatively impacts human health [*Ware et al.*, 1986; *Katsouyanni et al.*, 1997], causes acid rain [*Likens and Bormann*, 1974], and is oxidized in the atmosphere to produce sulfate aerosols (SA) that affect the global radiation budget and cloud microphysics [e.g., *Robock*, 2000; *von Glasow et al.*, 2009]. SA in the lower troposphere is efficiently removed (1–3 days) by wet and dry deposition producing mainly localized effects [*Chin et al.*, 2000; *Benkovitz et al.*, 2004]. Stratospheric SA, on the other hand, has a much longer lifetime (months to years) and can be transported long distances. SA reflects incoming solar radiation, thus causing Earth surface cooling [*Charlson et al.*, 1990]. In addition, SA provides surfaces for heterogeneous chemical reactions leading to stratospheric $O_3$ destruction [*Hofmann and Solomon*, 1989; *Brasseur and Granier*, 1992]. $SO_2$ is introduced into the atmosphere by natural sources (e.g., volcanic eruptions, oxidation of oceanic dimethyl sulphide (DMS) [*Berresheim et al.*, 1995]) and anthropogenic sources (e.g., fossil fuel burning (mostly coal) and metal smelting) [*Graf et al.*, 1997]. Although volcanic emissions account for only 10%–15% (15–21 Tg $SO_2$ [*Halmer et al.*, 2002]) of anthropogenic $SO_2$ emissions on an annual basis, volcanic eruptions can inject $SO_2$ directly into the free troposphere and stratosphere, with potentially significant climatic consequences [*Textor et al.*, 2003].

[3] The average mixing ratio of $SO_2$ in the free troposphere away from polluted regions is estimated at 15–100 ppt [*Thornton et al.*, 1997, 1999]. Continental concentrations in the planetary boundary layer (PBL) depend mainly on anthropogenic emissions and range from 20 ppt to hundreds of ppb [*Seinfeld and Pandis*, 1998]. Anthropogenic emissions vary globally due to economic development and differences in national environmental regulations. $SO_2$ emissions in the United States, Canada, and Europe decreased significantly over the past 30 years mainly due to strict regulations (e.g., 1970 and 1990 Clean Air Act Amendments in the United

[1]Laboratory for Atmospheric Research, Department of Civil and Environmental Engineering, Washington State University, Pullman, Washington, USA.
[2]Department of Geological and Mining Engineering and Sciences, Michigan Technological University, Houghton, Michigan, USA.
[3]Goddard Earth Sciences and Technology Center, University of Maryland Baltimore County, Baltimore, Maryland, USA.
[4]Joint Center for Earth Systems Technology, University of Maryland Baltimore County, Baltimore, Maryland, USA.


0148-0227/10/2009JD013492

States) [*Holland et al.*, 2000; *Stern*, 2005; *Giannitrapani et al.*, 2006, 2007; *Berglen et al.*, 2007]. On the other hand, anthropogenic emissions in Asia (e.g., China and India) have been increasing rapidly until recently due to economic growth and lack of emission controls [*Ta et al.*, 2005; *Kato and Akimoto*, 2007]. Careful monitoring of $SO_2$ emissions from natural and anthropogenic sources, $SO_2$ transport, and troposphere-stratosphere exchange are crucial for our understanding of sulfate aerosol formation and long-range transport leading to climatic effects [*Dickerson et al.*, 2007].

[4] Ground-based remote measurements of volcanic $SO_2$ fluxes started in early 1970s with the application of the correlation spectrometer (COSPEC) to volcano monitoring and volcanic risk assessment [*Moffat and Millan*, 1971; *Hoff and Millan*, 1981; *Andres*, 2001]. In recent years COSPEC has been gradually superseded by other remote sensing techniques such as Fourier transform infrared spectroscopy (FTIR) [*Oppenheimer et al.*, 1998; *Horrocks et al.*, 2001] and differential optical absorption spectroscopy (DOAS) [e.g., *Noxon*, 1975; *Platt*, 1994; *Platt and Stutz*, 2008]. Numerous DOAS instrument configurations have been deployed relying on artificial light sources (long-path DOAS) [e.g., *Kern et al.*, 2008] and direct [*Sommer* 2008] and scattered sunlight (passive DOAS). Different scanning observation geometries were developed using scattered sunlight to optimize flux measurements and plume characterization (scanning DOAS [*Edmonds et al.*, 2003; *Galle et al.*, 2003, 2005, 2009; *Bobrowski and Platt*, 2007; imaging DOAS: *Louban et al.*, 2009]). So-called mini-DOAS instruments are gaining more popularity due to their low cost, low power consumption, small size, and greater flexibility in observation geometries [*Galle et al.*, 2009]. Brewer spectrophotometers also measure $SO_2$, even though the instruments are optimized for ozone monitoring [*Kerr*, 2002]. Since the Brewer spectrophotometers are used for routine measurements of $O_3$ throughout the world (e.g., the Canadian stratospheric ozone and UV monitoring program, with 12 sites) [*Fioletov et al.*, 2008] they allow for occasional identification of transient volcanic plumes [*Krueger et al.*, 2000; *Fioletov et al.*, 1998].

[5] Several DOAS instrument networks have been deployed to continuously measure trace gases in close proximity (5–15 km) to active volcanoes at high time resolution (~5 min). Among these are the FLAME (flux automatic measurements) network installed on Mt. Etna and Mt. Stromboli, Italy in 2004 [*Salerno et al.*, 2009; *Burton et al.*, 2009], and networks at Soufrière Hills volcano, Montserrat [*Edmonds et al.*, 2003; *Rodríguez et al.*, 2008], and White Island, New Zealand [*Miller et al.*, 2006]. The most recent effort (2004–2009) was made by the Network for Observation of Volcanic and Atmospheric Change (NOVAC) project that includes 24 volcanoes (with potential expansion) located in Africa, Europe, and South and Central America (for more details, see *Galle et al.* [2009]). The main products of these measurements are gaseous fluxes emitted by the volcanoes. Flux calculations involve several steps including spectroscopic evaluation, vertical gas column conversion, and wind speed and plume geometry estimation [e.g., *Edmonds et al.*, 2003]. The accuracy of these measurements therefore depends on instrument properties (e.g., stray light, spectral and temporal sampling, temperature stability), and the observational conditions of each measurement (e.g., aerosol properties, loading, and profile) [*Kern et al.*, 2009]. Improvements in instrument quality and data interpretation will provide opportunities for satellite instrument validation using the flux measurements mentioned above.

[6] Satellite observations of volcanic $SO_2$ emissions began with observation of the 1982 El Chichon eruption cloud by the total ozone mapping spectrometer (TOMS) flown on the Nimbus-7 spacecraft [*Krueger*, 1983; *Krueger et al.*, 2008]. Several versions of the TOMS instrument have been deployed and the observations have resulted in a long-term volcanic $SO_2$ database covering the period from 1978 to 2005 [*Bluth et al.*, 1993; *Krueger et al.*, 2000; *Carn et al.*, 2003]. All magmatic eruptions greater than 5 kT (0.005 Tg) were detected with the TOMS instruments, but most volcanic degassing was below the retrieval noise level due to limited wavelength coverage and spatial resolution [*Carn*, 2004]. Recently developed hyperspectral satellite instruments such as the Global Ozone Monitoring Experiment (GOME) aboard ERS-2 since 1995 [*Burrows et al.*, 1999; *Thomas et al.*, 2005; *Khokhar et al.*, 2005], the Scanning Imaging Absorption Spectrometer for Atmospheric Cartography (SCIAMACHY) aboard ENVISAT since 2002 [*Bovensmann et al.*, 1999], and GOME-2 aboard MetOp-A since 2006 show greatly improved $SO_2$ sensitivity [*Eisinger and Burrows*, 1998; *Bramstedt et al.*, 2004; *Richter et al.*, 2006; *Lee et al.*, 2008]. However, their low spatial and temporal resolution (GOME: 40 × 320 $km^2$ with 3 day global coverage; SCIAMACHY: 30 × 60 $km^2$ at nadir with 6 day global coverage, GOME-2: 80 × 40 $km^2$ and with ~1 day global coverage) and lack of contiguous coverage still limit opportunities for detection of transient volcanic and pollution events.

[7] The Dutch-Finnish ozone monitoring instrument (OMI) [*Levelt et al.*, 2006], launched on the EOS/Aura platform in July 2004, offers better ground resolution (13 × 24 $km^2$ at nadir) and contiguous daily global coverage of transient $SO_2$ plumes due to its wide ground swath (2600 km) [*Krotkov et al.*, 2006; *Yang et al.*, 2007; *Carn et al.*, 2007; *Krotkov et al.*, 2008; *Yang et al.*, 2009]. The OMI $SO_2$ measurements require validation against ground-based and aircraft observations to ensure high-quality $SO_2$ data for climate and air quality modeling. The first attempt to validate OMI measurements of anthropogenic $SO_2$ in the PBL over NE China was reported by *Krotkov et al.* [2008]. In situ aircraft measurements using a pulse-florescence detector were compared to OMI tropospheric $SO_2$ retrievals. The air mass–corrected collection 3 OMI $SO_2$ retrievals agreed with the in situ aircraft data to within 1 Dobson unit (DU; 1 DU = $2.69 \times 10^{16}$ molecules/$cm^2$ = 0.029 g/$m^2$). Validation of $SO_2$ measurements in volcanic clouds is important, as $SO_2$ column amounts are typically much higher than those encountered in polluted regions, and hence correlative data provide feedback on $SO_2$ algorithm performance at high concentrations. However, the unpredictable nature of volcanic eruptions and volcanic cloud trajectories, and cloud inhomogeneity makes such validation logistically challenging, and opportunities are rare. A chance occasion to validate TOMS $SO_2$ data occurred when a $SO_2$ cloud produced by an Alaskan volcanic eruption (Mt. Spurr, 17 September 1992) drifted over a ground-based Brewer spectrophotometer in Toronto [*Fioletov et al.*, 1998; *Krueger et al.*, 2000]. A Toronto-based Brewer instrument also detected $SO_2$ in

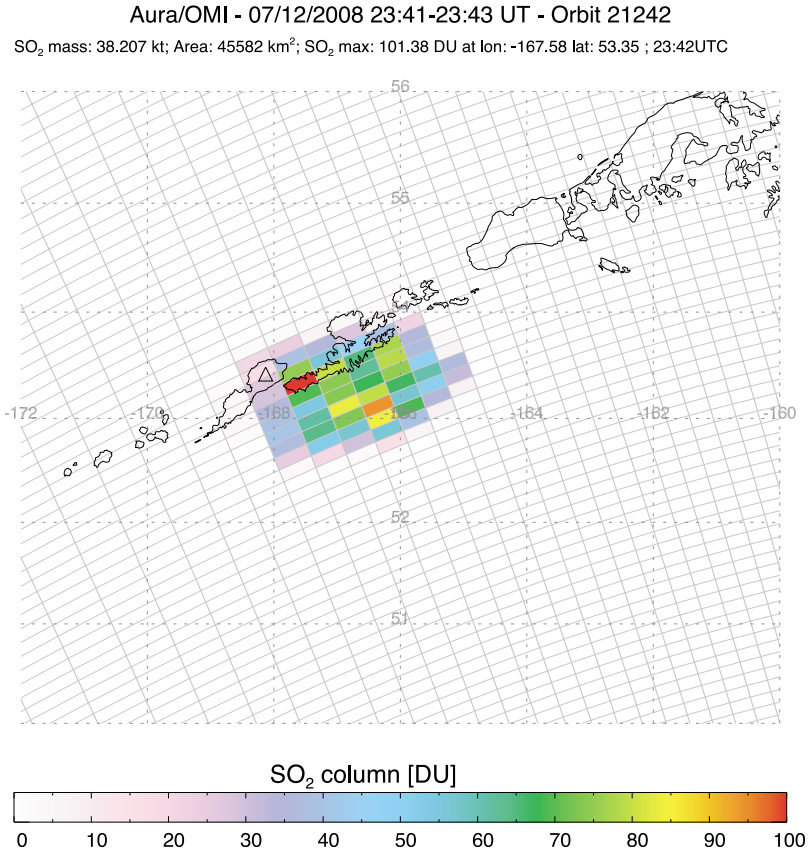


**Figure 1.** The Okmok $SO_2$ cloud as observed by OMI on 12 July 2008 at 23:42 UTC. The $SO_2$ columns shown are derived from the operational OMI linear fit algorithm [*Yang et al.*, 2007] assuming a $SO_2$ cloud center of mass altitude (CMA) of 17.5 km. Okmok volcano is indicated by a triangle. The maximum $SO_2$ column measured in the volcanic cloud at this time was 101.38 DU; observed east of the volcano at 53.35°N, 167.58°W.

the eruption cloud released by Mt. St. Helens (WA) in May 1980, while a Brewer instrument in Norrkoeping, Sweden detected a drifting $SO_2$ cloud produced by Krafla (Iceland) in September 1984 [*Kerr and Evans*, 1987]. Coincident TOMS and Brewer $SO_2$ columns agreed to within 20% in the 1992 Spurr eruption cloud. Until 2008, the Mt. Spurr eruption was the most recent case of a large volcanic eruption cloud drifting over the conterminous United States and Canada. Such events provide rare opportunities to observe volcanic cloud constituents from the ground and validate satellite retrievals. In 2008, major eruptions of two Alaskan volcanoes (Okmok and Kasatochi; both in the Aleutian Islands) produced extensive $SO_2$ clouds that drifted over North America. In this paper, we present the first robust comparison of OMI volcanic $SO_2$ retrievals with ground-based observations of the Okmok volcanic cloud at Washington State University (WSU) in Pullman, WA (46.73°N, 117.169°W) for Aura satellite overpasses during 18–20 July 2008. This successful validation was achieved using direct Sun measurements made by the multifunction differential optical absorption spectroscopy (MFDOAS) instrument developed at WSU [*Herman et al.*, 2009], which is capable of retrieving $SO_2$ columns with high precision (<0.2 DU). We begin section 2 by briefly describing the Okmok volcanic eruption (12 July 2008) and volcanic cloud transport as observed by OMI. Section 3 describes the ground-based MFDOAS and OMI retrieval methodology with a detailed discussion of data analysis and error estimation. In section 4, we compare MFDOAS data with operational and off-line OMI $SO_2$ products for 3 days in July 2008.

## 2. The Okmok Volcanic Eruption, 12 July 2008

[8] Okmok volcano, located on Umnak Island in Alaska (Aleutian Islands, 53.397°N, 168.166°W, altitude 1073 m), erupted unexpectedly and explosively on 12 July 2008 (11:43 Alaskan Daylight Time [ADT]). The eruption began with two explosions ~1 h apart that both reached the stratosphere. During the first explosion an opaque tephra-rich column reached 15 km altitude; the second explosion injected a more water vapor–rich column up to 16 km [*Larsen et al.*, 2009; *Neal et al.*, 2009]. The Okmok eruption continued for 5 weeks, during which ash and steam plumes were released continuously to altitudes of 2–12 km [*Larsen et al.*, 2009].

[9] The Okmok volcanic cloud, injected into the stratosphere by the initial explosions, contained high concentrations of $SO_2$ (column amounts up to ~100 DU or ~ 3 g/m$^2$ in the fresh plume) that were detected by several satellite instruments (e.g., AIRS, SCIAMACHY, GOME-2, OMI;

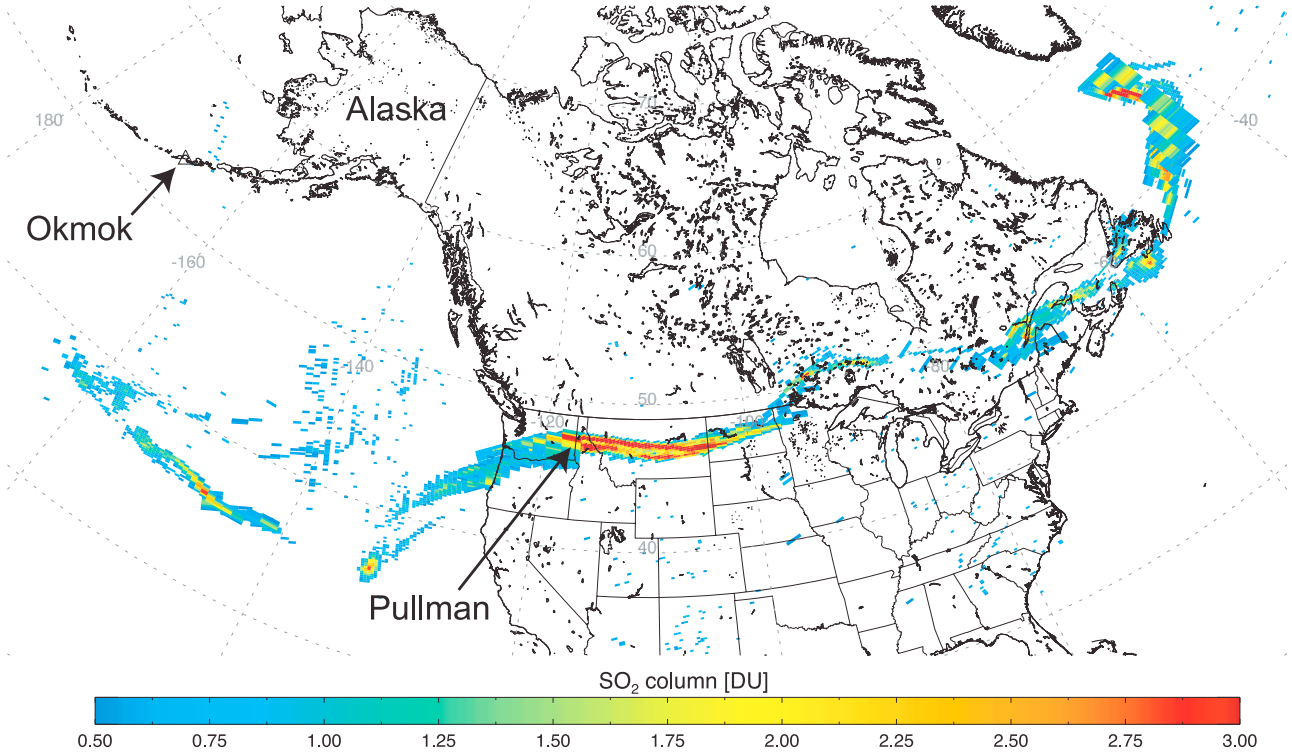


**Figure 2.** The Okmok $SO_2$ cloud as observed by OMI on 19 July 2008 between 15:35 and 23:50 UTC. The image is a composite of several contiguous OMI orbits. The $SO_2$ columns shown are derived from the operational OMI linear fit algorithm [*Yang et al.*, 2007] assuming a $SO_2$ cloud CMA of 17.5 km. The ground-based observations were made from Pullman, WA.

Figure 1 and Table 1). According to OMI measurements a total of ~0.1–0.2 Tg $SO_2$ was injected into upper troposphere and lower stratosphere (UTLS: 10–17 km, see Table 1). Until 16 July, the volcanic cloud was transported slowly south and east of the Aleutian Islands across the Gulf of Alaska. It then became entrained in the westerly jet stream and drifted over Washington State late on 16 July, before being sheared into an elongated banner extending across the entire North American continent on 18–20 July. By this time significant shearing of the volcanic cloud coupled with conversion of $SO_2$ to sulfate aerosol had reduced peak $SO_2$ column amounts to ~20 DU (Table 1). North-south movement of the jet stream produced several transits of the $SO_2$ cloud over the MFDOAS instrument in Pullman, WA during 18–20 July. Figure 2 shows the Okmok $SO_2$ cloud spread across North America on 19 June 2008 as measured by OMI.

[10] In total, OMI tracked the Okmok $SO_2$ plume for nearly 2 weeks as it drifted beyond North America, over the North Atlantic Ocean to Northern Europe. Large amounts of ash emitted by the initial eruptions fell out rapidly in the first couple of days. OMI monitored the amount of volcanic ash qualitatively using the aerosol index (AI) [*Yang et. al.*, 2010, this issue]. According to Geostationary Operational Environmental Satellite (GOES-West and East) [*Schreiner et al.*, 2001] visible and infrared imagery, the 5 day old volcanic cloud contained low levels of ash as it moved across the Pacific Northwest on 17 July. Cloud-Aerosol Lidar and Infrared Pathfinder Satellite Observation (CALIPSO) [*Hunt*

**Table 1.** OMI $SO_2$ Measurements for the Okmok Volcanic Cloud

| Date: July 2008 | OMI Orbits | Area $10^6$ ($km^2$)[a] | Peak $SO_2$ (DU)[b] | OMI $SO_2$ Mass (Tg)[c] |
|---|---|---|---|---|
| 12 | 21242 | 0.05 | >100 | 0.04 |
| 13 | 21256–21257 | 0.3–0.4 | 40–60 | ~0.1 |
| 14 | 21258–21271 | 0.8 | 35–42 | 0.12 |
| 15 | 21272–21286 | 0.9 | 30–32 | 0.079–0.091 |
| 16 | 35°N–55°N; 120°W–160°W | 0.9 | 26–32 | 0.075–0.083 |
| 17 | 35°N–60°N; 60°W–160°W | 1 | 21–23 | 0.067–0.075 |
| 18 | 35°N–60°N; 60°W–160°W | 1.1 | 22–28 | 0.054–0.063 |
| 19 | 30°N–65°N; 35°W–175°W | 1.17 | 6–8 | 0.041–0.051 |

[a]Total area of OMI pixels comprising the Okmok $SO_2$ cloud.
[b]Collection 3 operational OMSO2 data for $SO_2$ distributed between 5 and 20 km (center of mass altitude (CMA) of 7.5–17.5 km).
[c]$SO_2$ mass derived from OMI observations.

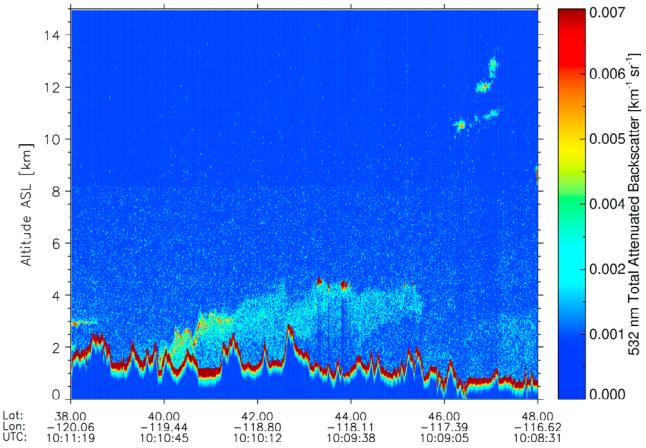


**Figure 3.** CALIPSO 532 nm total attenuated backscatter profile over the western United States at ~10:10 UTC on 18 July 2008. Sulfate aerosol in the 1 week old Okmok volcanic cloud is evident at altitudes of 10–13 km at 46°N–48°N. Elevated lidar returns at lower altitudes are plumes from forest fires in northern California.

*et al.*, 2009] measurements on 19 July also showed low levels of ash in the 1 week old Okmok cloud.

## 3. Data Collection

### 3.1. OMI Data

[11] OMI was launched on NASA's Aura spacecraft in July 2004 and circulates in a Sun-synchronous orbit at 705 km altitude providing daily global coverage with a spatial resolution of 13 km (along track) × 24 km (across track) at nadir and lower resolution at off-nadir look angles on its 2600 km swath. OMI makes hyperspectral measurements of solar irradiance and backscattered Earth radiance in the UV and VIS channels (270–500 nm) using two 2-D charge-coupled device (CCD) detectors with an average spectral resolution of 0.5 nm. The 2-D CCD (576 × 780 pixels) allows simultaneous spectral and cross-track spatial measurements for the first time. One CCD dimension (576 cross-track pixels) provides spatial information, while the other dimension (780 pixels) supplies spectral information. Advances in CCD technology and OMI's optical design have resulted in unprecedented sensitivity to $SO_2$ and other trace gases (e.g., $NO_2$, $O_3$, BrO, OClO, and HCHO) [*Levelt et al.*, 2006]. Improvements in OMI $SO_2$ retrieval algorithms have permitted detection of $SO_2$ emissions and transport from volcanic eruptions and passive degassing, coal-burning power plants and metal smelters [e.g., *Carn et al.*, 2007, 2008a, 2008b; *Krotkov et al.*, 2008].

[12] Operationally, volcanic $SO_2$ total columns are retrieved from OMI's UV-2 subchannel (310–365 nm) using a linear fit (LF) algorithm [*Yang et al.*, 2007]. The LF algorithm simultaneously retrieves vertical columns of $SO_2$, $O_3$, and effective surface reflectivity using 10 discrete bands in regions of strong and weak absorption by $O_3$ (six bands) and $SO_2$ (four bands) [*Yang et al.*, 2007]. The retrieval is based on interpolation of look-up tables, precomputed using a forward radiative transfer model (TOMRAD) as a function of TOMS-V8 climatological ozone and temperature profiles [*Bhartia and Wellemeyer*, 2004], viewing geometry and OMI-derived effective surface/cloud pressure [*Joiner and Vasilkov*, 2006]. The $SO_2$ vertical column retrieval depends on the assumed $SO_2$ profile shape, represented by its center of mass altitude (CMA). For volcanic clouds in the free troposphere and stratosphere, operational $SO_2$ columns (OMSO2) are provided for three different values of the CMA (lower troposphere [TRL], CMA = 3.5 km; midtroposphere [TRM], CMA = 7.5 km; and lower stratosphere [STL], CMA = 17.5 km). The altitude of the Okmok volcanic cloud was constrained using CALIPSO aerosol data [*Thomason and Pitts*, 2008; *Carn et al.*, 2008b]. The CALIPSO lidar detected sulfate aerosols in the volcanic cloud at altitudes of 10–13 km on 18 July 2008 (Figure 3). On the basis of the reasonable assumption that the $SO_2$ and sulfate aerosol were collocated, the $SO_2$ CMA was assumed to be 11.5 km with an error of ±1.5 km. Corresponding $SO_2$ columns were therefore calculated by linear interpolation between the operational TRM and STL retrievals to obtain the best $SO_2$ column estimate for each OMI scene.

[13] Assuming that the $SO_2$ cloud height is correct, residual biases in the operational LF retrievals due to latitude and viewing angle are ~0.1 DU [*Yang et al.*, 2007]. The error in the OMI $SO_2$ retrieval due to the uncertainty in the actual CMA (±1.5 km) is approximately 5% of the $SO_2$ vertical column density (VCD). The OMI pixel noise standard deviation (precision) is about 0.2–0.3 DU. Systematic errors due to nonlinear $SO_2$ absorption effects are negligible when $SO_2$ loading is less than ~30 DU and no ash is present [*Yang et al.*, 2007], as was the case for the Okmok cloud over Pullman. An off-line nonlinear iterative spectral fitting (ISF) $O_3$/$SO_2$ retrieval [*Yang et al.*, 2009] was also performed assuming a Gaussian $SO_2$ vertical profile with a full width at half maximum (FWHM) of 3 km centered at 11.5 km altitude and adjusted using the average background $SO_2$ amount for each OMI cross-track position. Both LF (OMSO2) and ISF $SO_2$ retrievals were compared with the ground-based direct Sun MFDOAS measurements.

### 3.2. Ground-Based MFDOAS Data

#### 3.2.1. MFDOAS Description

[14] The MFDOAS was designed as a research grade instrument to measure spectral UV/VIS direct Sun (DS) irradiance and scattered sky (SS) radiance for atmospheric trace gases retrievals. Spectra are recorded by the spectrometer/CCD system with a spectral resolution of 0.83 nm (sampling of 7.8 pixels per FWHM) and cover the 281–498 nm wavelength region. Instrumental fields of view for scattered and direct sunlight are 1° × 0.5° and 1° respectively. Direct sunlight is guided into a spectralon integrating sphere where multiple scattering within the sphere reduces the solar intensity and assures uniform illumination of the spectrometer optics, thus minimizing effects of pointing errors. SS measurements can be taken at any azimuth and elevation angle allowing for multiaxis and zenith sky (ZS) observations. The instrument exhibits excellent signal-to-noise properties and sensitivity allowing for high time resolution measurements (exposures of a few seconds for DS and subsecond for SS). The signal-to-noise ratio (S/N) at small solar zenith angles (SZA) around the OMI overpass time is 1600–2100 at 307.5 nm and 3900–4200 at 327 nm for each spectral integration (no time averaging). This is achieved by coadding the signal from 400 rows of the

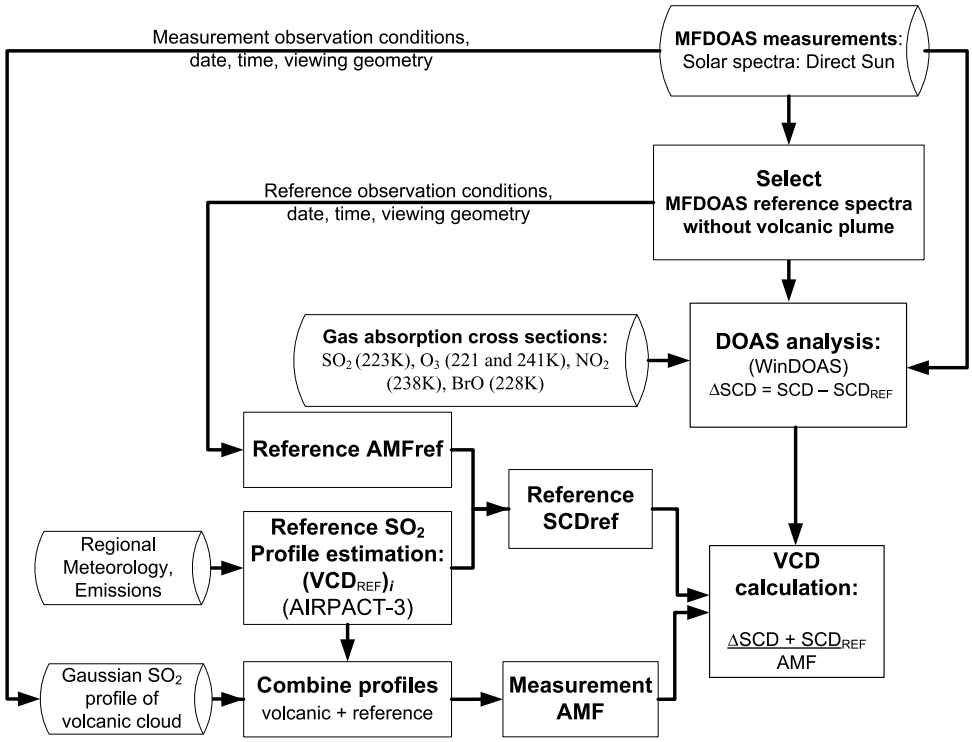


**Figure 4.** MFDOAS direct Sun data analysis flowchart.

UV-enhanced back-illuminated CCD (Princeton Instruments: PIXIS-2KBUV).

[15] The MFDOAS instrument made DS measurements continuously during daylight hours from 14:00 UTC on 18 July until 2:00 UTC on 22 July 2008. The Okmok volcanic cloud first drifted over Washington State on 16–17 July and fragments of the cloud remained overhead until 21 July. A narrowband UV filter (Hoya U340) was used to (nearly) eliminate the effects of unwanted stray light in the spectrometer system at shorter wavelengths. The CCD was thermoelectrically cooled to -70°C, while the spectrometer/CCD box was thermally controlled at 20°C ± 0.5°C. An average integration times in DS mode was 4 s.

### 3.2.2. MFDOAS Data Analysis

[16] Collected spectra were analyzed using the DOAS technique. The analysis consists of the following steps, also outlined in Figure 4:

[17] 1. DOAS analysis: calculation of $SO_2$ differential slant column densities (ΔSCD) relative to a background reference spectrum without volcanic $SO_2$ using the WinDOAS spectral least squares fitting program [*Van Roozendael and Fayt*, 2001];

[18] 2. Calculation of $SO_2$ slant column density in the background reference spectrum ($SCD_{ref}$):

[19] a. estimation of the background $SO_2$ concentration profile using the chemical air quality model AIRPACT-3 [*Chen et al.*, 2008],

[20] b. calculation of the air mass factor for the reference observation conditions ($AMF_{REF}$).

[21] 3. Calculation of the air mass factor for the measurement observation conditions (AMF);

[22] 4. Calculation of the $SO_2$ VCD: VCD = (ΔSCD + $SCD_{ref}$)/AMF.

#### 3.2.2.1. DOAS Analysis

[23] DOAS analysis of the collected spectra is based on the Beer-Lambert law (BLL) [e.g., *Platt*, 1994; *Platt and Stutz*, 2008]. Solar light attenuation in the atmosphere, described by the BLL equation (1), is due to molecular and aerosol absorption and scattering by air molecules (Rayleigh) and aerosols (Mie),

$$I(\lambda) = Io(\lambda) \cdot \exp\left\{-\left[\sum_i (\sigma_i(\lambda)\cdot c_i)\cdot L + \varepsilon_R(\lambda)\cdot L + \varepsilon_M(\lambda)\cdot L\right]\right\}, \quad (1)$$

where $I(\lambda)$ and $Io(\lambda)$ are the intensities of an attenuated and a reference spectrum [counts] at a wavelength $\lambda$, $\sigma_i(\lambda)$ is the temperature- and pressure-dependent absorption cross section of molecular species $i$ [$cm^2$/molecule] at wavelength $\lambda$, $c_i$ is the number density of species $i$ [molecules/$cm^3$], $\varepsilon_R(\lambda)$ and $\varepsilon_M(\lambda)$ are Rayleigh and aerosol (Mie) extinction coefficients [$cm^{-1}$] respectively, and $L$ is an average photon path [cm]. The DOAS technique takes advantage of the strong wavelength dependence of the differential absorption structure of molecular absorption cross sections ($\sigma'_i(\lambda)$) to separate trace gas species in the atmosphere. The BLL equation (1) transforms into the DOAS BLL equation (2).

$$\log(I(\lambda)) - \log(Io(\lambda)) = -\left\{\underbrace{\left[\sum_i \left(\sigma'_i(\lambda)\cdot \mathrm{SCD}_i\right)\right]}_{\text{dif absorption}} + \underbrace{\left[\sum_i \sigma_{i0}(\lambda)\cdot c_i + \varepsilon_R(\lambda) + \varepsilon_M(\lambda)\right]\cdot L}_{\text{wide band extinction}}\right\} \quad (2)$$

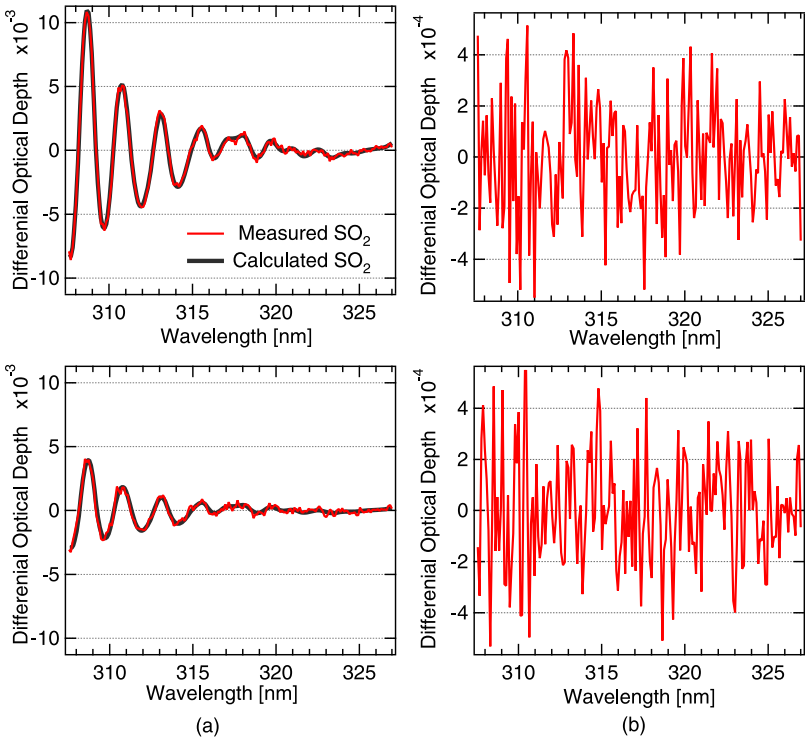


**Figure 5.** (a) $SO_2$ differential optical depth and (b) fitting residual optical depth for high (top, 20:29 UTC 19 July 2008) and low (bottom, 21:12 UTC 20 July 2008) Okmok volcanic cloud $SO_2$ concentrations from MFDOAS direct Sun measurements over Pullman, WA.

The DOAS spectral fitting procedure involves the simultaneous least squares fitting of slant column densities ($SCD_i = c_iL$ in (2)) of various molecular absorbers and a low-order polynomial function to the difference between the logarithms of the attenuated and reference spectra. A low-order polynomial ($P_{LO}$) is used to account for wideband extinction due to Rayleigh and Mie scattering and molecular absorption that is only weakly wavelength-dependent $\sigma_{i0}(\lambda)$. Measured and reference spectra are first corrected for dark current, stray light, and pixel-to-pixel sensitivity. The MFDOAS detector dark current is very low due to CCD cooling to −70°C and short integration times. The stray light signal is also low due to application of the filter absorbing visible light (>400 nm) where the solar intensity peaks. The spectra are further aligned to correct for any wavelength shift between the spectra due to instrument motion and small temperature changes. In addition, a small offset is applied to the measured spectra to correct for any residual stray-light and dark signal. Equation (3) is a simplified form of (2) [*Van Roozendael and Fayt*, 2001],

$$\log[I(\lambda) - \text{offset}(\lambda)] - \log[Io(\lambda)] = -\sum_i \left[\sigma_i'(\lambda)_{\text{instrument}} \cdot \text{SCD}_i\right] - P_{\text{LO}}, \quad (3)$$

where $\sigma_i'(\lambda)_{\text{instrument}}$ $SCD_i$ is the differential optical depth due to species $i$. Note that the SCD calculated by the DOAS technique is determined relative to the absorber amount in the reference spectrum $I_o(\lambda)$. For satellite instruments, where the extraterrestrial solar reference spectrum is measured, the DOAS technique produces an absolute SCD ($SCD_{ABS}$). For a passive ground-based DOAS technique, a reference spectrum is typically measured under the minimum attenuation conditions possible for the molecular absorber of interest (shortest photon path and lowest molecular absorber column). The reference spectrum in this study was taken at 19:20 UTC (11:20 local time) on 21 July 2008, when the Okmok $SO_2$ cloud was not present over Pullman, WA, providing spectra containing no volcanic $SO_2$ absorption.

[24] $SO_2$ differential slant column densities (ΔSCD) were calculated using WinDOAS [*Van Roozendael and Fayt*, 2001] in the 307.5–327 nm wavelength region. The wavelength cutoff at 307.5 nm was chosen to ensure S/N of at least 850 at large SZAs. The fitting window was extended to 327 nm (beyond the region of strong $SO_2$ absorption) to minimize the correlation coefficient between ozone and $SO_2$ absorption cross sections. Sensitivity studies were performed to evaluate the effect of the chosen fitting window on the $SO_2$ retrieval, e.g., expansion of the fitting window to 301–327 nm to include additional $SO_2$ absorption bands resulted in slightly smaller $SO_2$ ΔSCD (<1.2%), well within the measurement/analysis error.

[25] $SO_2$ (223 K), $O_3$ (221 and 241 K), $NO_2$ (238 K), BrO (228 K) differential absorption cross sections and a fourth-order polynomial were used as fitting parameters in equation (2). Higher resolution laboratory cross sections of $NO_2$ [*Vandaele et al.*, 1998], BrO [*Wilmouth et al.*, 1999], $SO_2$ [*Bogumil et al.*, 2003], and $O_3$ [*Malicet et al.*, 1995] at corresponding temperatures (see above) were convolved with the lower resolution MFDOAS instrument line shape

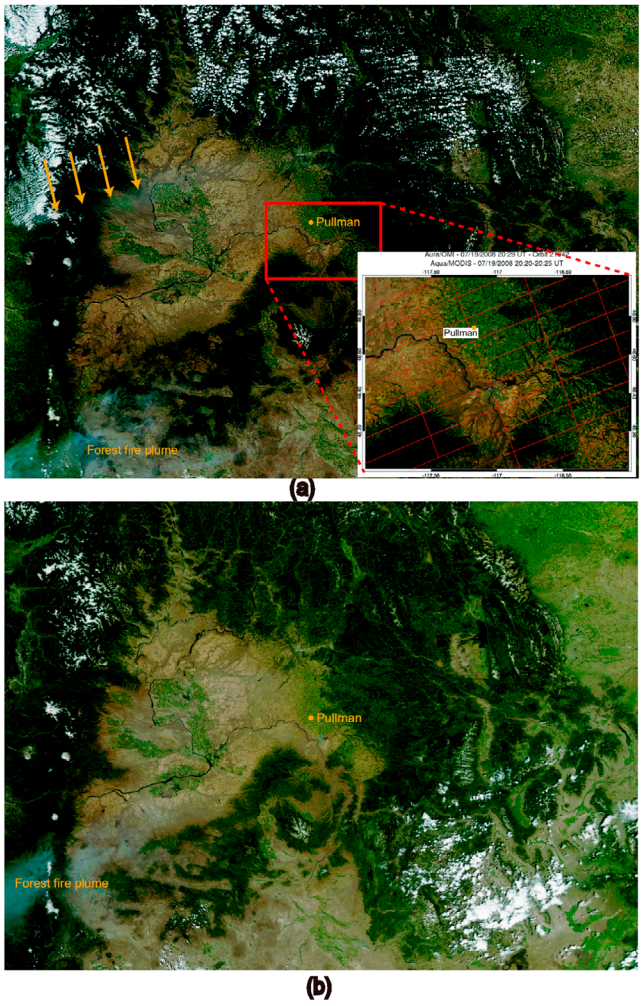


**Figure 6.** Aqua MODIS true color imagery (composites of MODIS visible bands 1, 4, and 3) of the Pullman region. (a) Aqua MODIS scene at 20:20 UTC on 19 July 2008. Inset shows OMI pixel boundaries in the region of Pullman for the 20:29 UTC OMI overpass. Arrows indicate northern edge of a faint band of haze, likely due to scattering by aerosol in the Okmok volcanic cloud. (b) Aqua MODIS scene at 21:00 UTC on 20 July 2008. Note the forest fire plume in the SW corner of both images (see Figure 3). Image dimensions are ~850 km (E-W) × 720 km (N-S). Images courtesy of the MODIS Rapid Response project, NASA/GSFC.

function to produce a cross section, characteristic of the measured atmospheric spectrum. In addition, $O_3$, $SO_2$, and $NO_2$ cross sections were *Io* corrected to account for differences between the "smooth" laboratory light source and the highly structured solar spectrum [*Aliwell et al.*, 2002]. An $SO_2$ temperature of 223 K was estimated based on radiosonde soundings near Spokane, WA (113 km north of Pullman) and the assumed altitude of the Okmok volcanic cloud (11.5 km). Because of the strong temperature dependence of ozone absorption cross sections in this wavelength region and the atmospheric vertical temperature variability across the ozone vertical profile, $O_3$ cross sections at 221 K and 241 K were fitted to the observed spectrum [*Aliwell et al.*, 2002; *Bernhard et al.*, 2005]. Figure 5 shows an example of the spectral fitting quality for high and low $SO_2$ columns during OMI overpass times.

#### 3.2.2.2. Calculation of $SO_2$ SCDref

[26] The $SO_2$ slant column in the reference spectrum ($SCD_{REF}$) was calculated according to equation (4):

$$SCD_{REF} = \sum_{BOA}^{TOA} (VMR_i \cdot \rho_{air_i} \cdot \Delta h_i \cdot AMF_i), \quad (4)$$

where $VMR_i$ is the volume mixing ratio of $SO_2$ in atmospheric layer $i$, $\rho_{air\ i}$ is the air density in layer $i$ [molecules/cm$^3$], $\Delta h_i$ is the layer height [cm], $AMF_i$ is the (box) AMF in layer $i$, and BOA and TOA are the bottom and top of the atmosphere, respectively. The $SO_2$ VMR profile at the time of the reference measurement was estimated using the AIRPACT-3 modeling system for the Pacific Northwest (http://www.airpact-3.wsu.edu). The AIRPACT-3 model accounts for nonvolcanic $SO_2$ emissions (including wild fires), meteorology, and chemistry in the Pacific Northwest. Gas volume mixing ratios are calculated for 21 atmospheric layers with varying layer height (~100 m below 1 km) up to ~15.5 km [*Chen et al.*, 2008]. We assume that $SO_2$ VMRs in layers above 15.5 km are equal to the VMR in the highest AIRPACT-3 layer.

[27] $AMF_i$ represents an enhancement in gas absorption due to a change in the photon path through layer $i$ compared to a vertical path through the layer. DS measurements at SZA < 60° are almost equally sensitive to absorption in all layers ($AMF_i \approx$ DS_AMF) and mainly depend on the SZA corrected for refraction (SZA*), the effective height of the $SO_2$ profile ($h_{eff}$), and the radius of the Earth at the measurement location ($R_{Earth}$). DS_AMF can be estimated geometrically using equation (5) [*Bernhard et al.*, 2005; *Cede et al.*, 2006; *Herman et al.*, 2009],

$$DS\_AMF = \sec\left\{\arcsin\left[\left(\frac{R_{Earth}}{R_{Earth} + h_{eff}}\right) \cdot \sin\left(SZA^*\right)\right]\right\}, \quad (5)$$

where $h_{eff}$ is the profile weighted layer height ($h_i$) calculated according to equation (6),

$$h_{eff} = \frac{\sum_{BOA}^{TOA} (VMR_i \cdot \rho_{air_i} \cdot \Delta h_i \cdot h_i)}{\sum_{BOA}^{TOA} (VMR_i \cdot \rho_{air_i} \cdot \Delta h_i)}. \quad (6)$$

DS_AMF exhibits only a small sensitivity to $h_{eff}$ at SZA < 60°. The difference between DS_AMF calculated for $h_{eff}$ of 1 and 20 km is < 0.6% at a SZA of 55°. Furthermore, the maximum SZA at OMI overpass times during passage of the Okmok volcanic cloud over Pullman was 37°, making MFDOAS DS_AMFs almost insensitive to the $SO_2$ profile.

[28] A reference $h_{eff}$ of 2.8 km was estimated using the $SO_2$ VMR profile modeled by AIRPACT-3. Interestingly, the AIRPACT-3 predicted elevated $SO_2$ concentrations above 3 km on 20 and 21 July, which may be indicative of the transport from wildfires in Northern California (Figures 3 and 6). The resulting $SCD_{REF}$ was 0.115 DU ± 100%. This value is within the range of reported concentrations for clean continental area [*Thornton et al.*, 1999; *U. S. EPA*, 2008].

**Table 2.** OMI Overpass Data for WSU MFDOAS Direct Sun Measurements

| Date: July 2008 | Time (UTC) | Orbit | xT[a] | OMILat[b] °N | OMI Lon[b] °W | OMI CF[c] | Operational OMI $SO_2$ (DU) 5KM[d] | 15KM[e] | Interp.[f] | ISF $SO_2$ (DU)[g] | DS MFDOAS $SO_2$ (DU)[h] |
|---|---|---|---|---|---|---|---|---|---|---|---|
| 18 | 19:47 | 21327 | 1 | 46.61 | 117.51 | 0 | 0.19 | 0.11 | 0.16 ± 0.22 | – | 0.18 ± 0.11 |
| 18 | 21:24 | 21328 | 48 | 46.75 | 117.30 | 0 | −0.24 | −0.17 | – | – | 0.18 ± 0.11 |
| 19 | 20:29 | 21342 | 11 | 46.81 | 116.96 | 0 | 3.35 | 2.58 | 3.04 ± 0.27 | 2.96 ± 0.27 | 3.11 ± 0.17 |
| 19 | 22:07 | 21343 | 60 | 46.70 | 117.54 | 0 | 1.63 | 0.93 | 1.35 ± 0.23 | 1.49 ± 0.24 | 1.75 ± 0.12 |
| 20 | 21:12 | 21357 | 41 | 46.68 | 117.10 | 0 | 1.16 | 0.86 | 1.04 ± 0.23 | 1.42 ± 0.24 | 1.22 ± 0.12 |

[a]OMI cross-track pixel number: 20–40 are nadir or near-nadir (13 × 24 $km^2$), 10–19 and 41–50 are off-nadir (>13 × 24 $km^2$), and 1–9 and 51–60 are far off-nadir (≫13 × 24 $km^2$).
[b]Lat, Lon corresponds to center of OMI pixel containing the MFDOAS location.
[c]OMI-derived radiative cloud fraction.
[d]Collection 3 operational OMSO2 data for $SO_2$ distributed between 5 and 10 km (CMA = 7.5 km).
[e]Collection 3 operational OMSO2 data for $SO_2$ distributed between 15 and 20 km (CMA = 17.5 km).
[f]5KM and 15KM OMSO2 data linearly interpolated to a volcanic cloud altitude of 11.5 km.
[g]Off-line iterative spectral fit (ISF) retrieval [*Yang et al.*, 2009], assuming a Gaussian $SO_2$ vertical profile with a FWHM of 3 km centered at 11.5 km altitude, and adjusted using the average background $SO_2$ amount for this OMI cross-track position.
[h]MFDOAS vertical column from DS measurements at the OMI overpass time (1 min average).

#### 3.2.2.3. Calculation of Measurement AMF

[29] Measurement AMFs were calculated in the same manner as the AMF for the reference spectrum. $SO_2$ profile for the volcanic cloud was described by a Gaussian function with a FWHM of 3 km centered at 11.5 km. DS_AMF was calculated assuming $h_{eff}$ = 11.5 km for the volcanic cloud location.

#### 3.2.2.4. Calculation of $SO_2$ VCD

[30] Differential slant columns (ΔSCD) calculated using the DOAS analysis were converted to VCDs by dividing the true slant column density (ΔSCD plus $SCD_{REF}$) by the corresponding AMF.

#### 3.2.2.5. MFDOAS Accuracy

[31] The error in the MFDOAS-retrieved DS $SO_2$ VCD ($\varepsilon_{SO2}$) combines errors in true slant column calculation and errors in AMF determination. $\varepsilon_{SO2}$ can be estimated by summing the corresponding errors in quadrature (equation (7)),

$$\varepsilon_{SO2} = \sqrt{\left(\frac{\varepsilon_{\Delta SCD}}{AMF}\right)^2 + \left(\frac{\varepsilon_{SCD_{REF}}}{AMF}\right)^2 + \left[\frac{\varepsilon_{AMF}(SCD_{REF} + \Delta SCD)}{AMF^2}\right]^2}. \quad (7)$$

Uncertainties in MFDOAS true (absolute) slant columns are mainly due to statistical errors of the DOAS fitting and systematic errors due to $SO_2$ absorption cross-section uncertainty, wavelength calibration, and errors in the approximation of $SCD_{REF}$. $SO_2$ absorption cross-section errors consist of uncertainty in the laboratory measured $SO_2$ cross section at 223 K (3%) [*Bogumil et al.*, 2003], uncertainty in the MFDOAS instrument line shape function and wavelength calibration (~1% error in retrieved ΔSCD), and error in the $SO_2$ cloud temperature. According to CALIPSO data, the volcanic cloud was located between 10 and 13 km on 18 July 2008 (Figure 3), and we assume a CMA of 11.5 km. Radiosonde temperature profiles from Spokane, WA indicated temperatures of 216–224 K at 11.5 km altitude during 18–21 July. An error in $SO_2$ cloud altitude (CALIPSO data are not available for 19–21 July) of ±1.5 km will result in a radiosonde observed temperature range of 215–234 K. This translates into an error of ±2% in retrieved $SO_2$ SCD. Statistical noise in the DOAS fitting was estimated using the WinDOAS program. Uncertainty in the reference column density calculated by the AIRPACT-3 system is estimated to be 0.11 DU (J. K. Vaughan, personal communication). Error in the direct Sun AMFs is less than 1% for the SZA conditions prevailing during the volcanic cloud measurements (the maximum SZA with acceptable S/N was 60°). SZAs during OMI overpasses varied between 26° and 37.5°. The overall error in $SO_2$ VCD depends on the measured ΔSCD and is estimated to be between 5.5 % and 9.8 % during OMI overpass times (Table 2).

## 4. Results and OMI Validation

[32] Meteorological conditions were very favorable for DS-MFDOAS and satellite observations during the Okmok volcanic cloud passage over Pullman, WA (18–20 July 2008). On the basis of GOES and Moderate Resolution Imaging Spectroradiometer (MODIS) [*Justice et al.*, 2002; *Platnick et al.*, 2003] observations, eastern Washington was almost cloud-free for the entire period (Figure 6). The

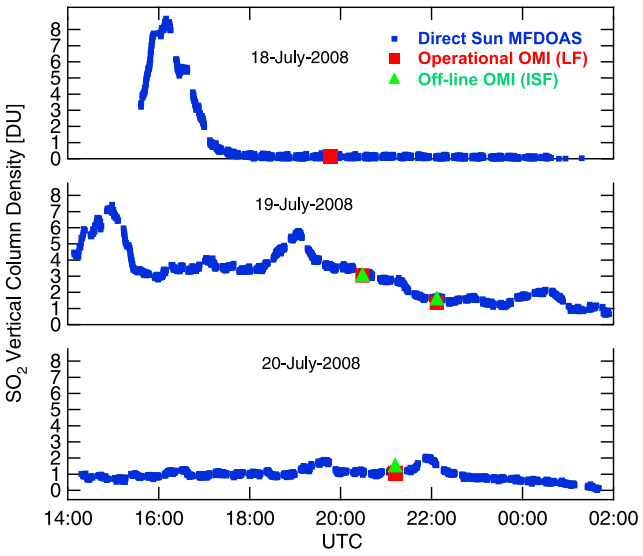


**Figure 7.** Time-series of direct Sun $SO_2$ VCDs measured by the WSU MFDOAS during transit of the Okmok volcanic cloud, with corresponding OMI overpass data (Table 2).

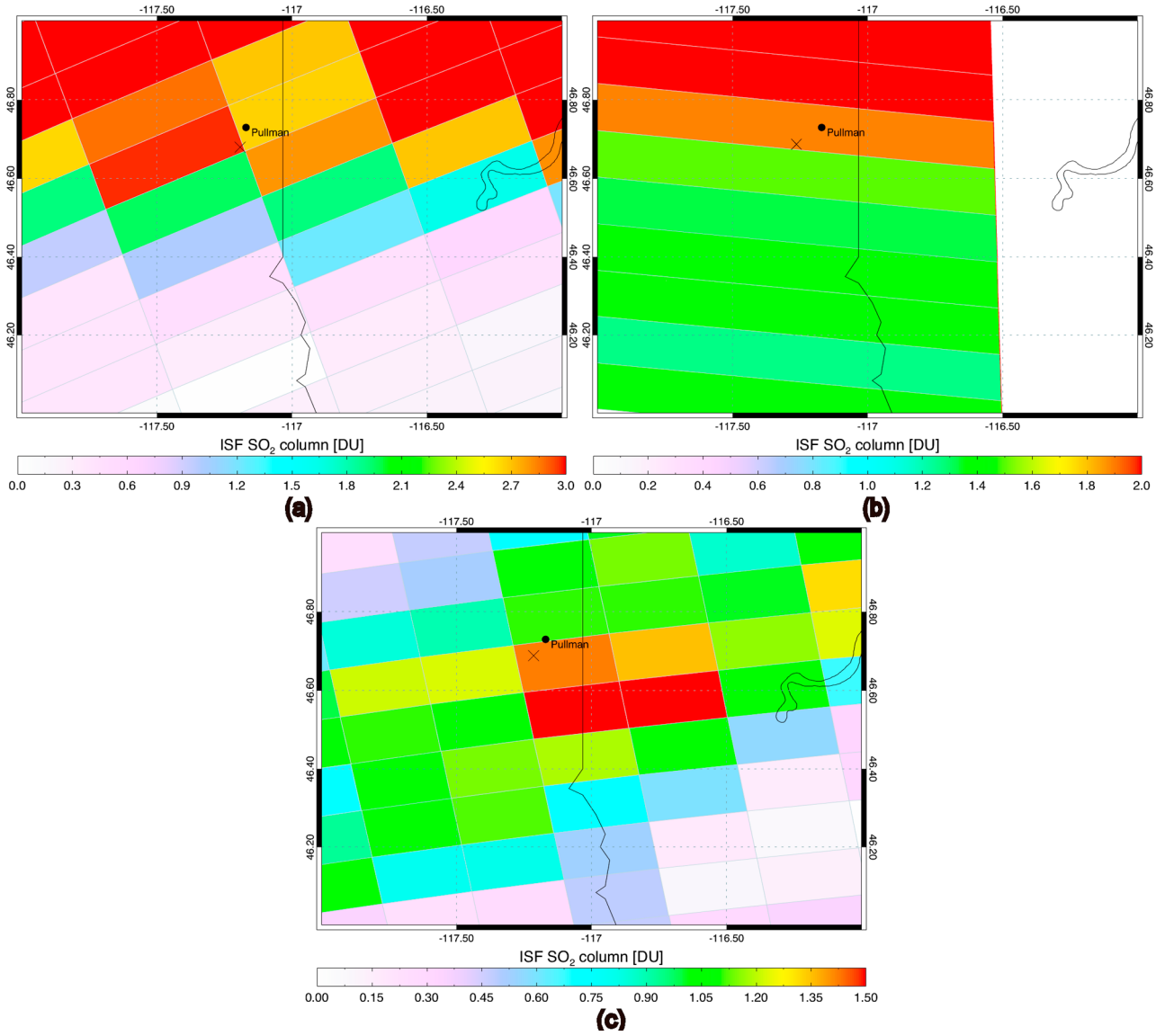


**Figure 8.** OMI ISF $SO_2$ retrievals for the Okmok volcanic cloud over WSU (a) 19 July 2008 at ~20:29 UTC, (b) 19 July 2008 at ~22:07 UTC, and (c) 20 July 2008 at 21:12 UTC. The location of Pullman, WA (WSU) is indicated. The cross indicates the location of the $SO_2$ VCD measured by direct Sun MFDOAS based on the solar zenith and azimuth angle at the time of the OMI overpass and a $SO_2$ cloud altitude of 11.5 km.

radiative cloud fraction in the OMI pixels over Pullman during the validation period was zero (Table 2). Figure 7 shows the complete DS-MFDOAS data set for the Okmok volcanic cloud passage over WSU, with the corresponding OMI overpass data; the latter are also shown in Table 2. Because of the movement of the jet stream north and south of Pullman, there were no coincident OMI and MFDOAS measurements of $SO_2$ VCDs above background levels at the MFDOAS location until 19 July. The maximum $SO_2$ column detected by the continuous daytime MFDOAS measurements was ~9 DU on 18 July (16:10 UTC). On the same day, however, the volcanic cloud shifted south of Pullman and MFDOAS measured background $SO_2$ concentrations for the rest of the day. OMI measured background $SO_2$ amounts (<0.2 DU) over Pullman at 19:47 and 21:24 UTC on 18 July (Figure 7 and Table 2). On 19 July, the $SO_2$ cloud was again within the MFDOAS field of view. The $SO_2$ VCD changed somewhat rapidly in the first part of the day (~4 DU/h from 7:00 to 8:00 and ~3.2 DU/h from 10:15 to 11:00 (PST)) and steadily declined in the afternoon. MFDOAS measured 3.11 ± 0.23 DU during the first OMI overpass (20:29 UTC) and 1.75 ± 0.16 DU during the second overpass (22:07 UTC) (Table 2). On 20 July, $SO_2$ column amounts remained low (1.22 ± 0.18DU at 21:12) with little temporal and spatial variability (Figure 7) as the tail-end of the sheared-out $SO_2$ cloud passed overhead.

### 4.1. MFDOAS and OMI Comparison

[33] Comparing ground-based measurements to satellite observations for transient volcanic clouds poses a problem

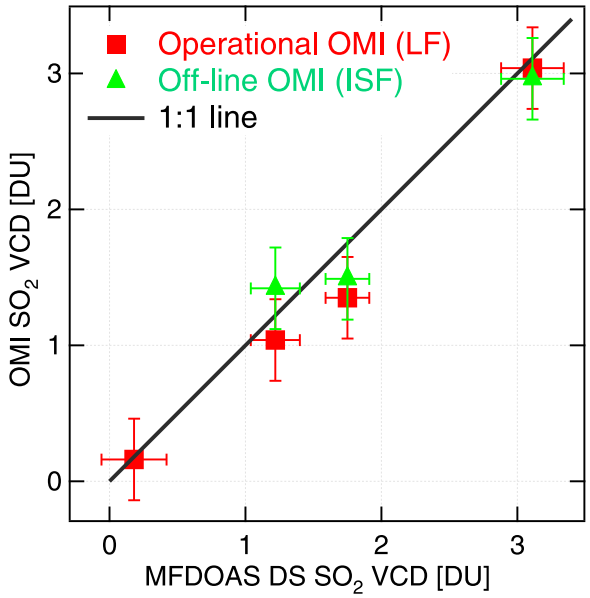


**Figure 9.** Correlation between OMI $SO_2$ retrievals and ground based direct Sun MFDOAS measurements in the Okmok volcanic cloud over Pullman, WA (18–20 July, 2008).

due to the differences in spatial averaging and cloud heterogeneity. In situ measurements of the stratospheric volcanic cloud produced by Hekla (Iceland) in 2000 showed significant $SO_2$ concentration variations on horizontal scales of 5–10 km [*Rose et al.*, 2006], which is smaller than an OMI pixel. However, we note that in the Hekla encounter the volcanic cloud was only sampled at one altitude, and so concentration variations along the aircraft flight path do not necessarily translate into spatial variations in $SO_2$ total column.

[34] In the case of the Okmok volcanic cloud, we have no ancillary data on the vertical distribution of $SO_2$. A direct Sun ground-based (DS-GB) instrument "samples" a narrow (1° FOV) conical air mass along the path of nonscattered solar photons. The actual area sampled by the DS-GB measurements, as seen from space, depends on the SZA, and on the altitude and thickness of the volcanic cloud. We estimate that on average a ~1.5 × 0.15 $km^2$ area of the volcanic cloud was sampled by MFDOAS during OMI overpasses. This is a small fraction of the OMI near nadir pixels (13 × 24 $km^2$). If any horizontal and/or vertical heterogeneity is present, comparison between the ground-based and satellite retrievals can be misleading. However, the measurements were made a number of days after the eruption, and we contend that progressive shearing of the volcanic cloud into a thin layer during transport would have substantially homogenized the horizontal and vertical $SO_2$ distribution.

[35] For comparison with DS-MFDOAS observations, OMI ground pixels were carefully selected to account for spatial sampling of the volcanic $SO_2$ cloud by the MFDOAS instrument. The approximate position of the volcanic cloud sampling was calculated from the solar zenith and azimuth angles during each OMI overpass, using the assumed Okmok cloud altitude of 11.5 km. Figure 8 shows the OMI pixel boundaries and DS-MFDOAS plume sampling locations on 19 and 20 July 2008. The best spatial coincidence occurred on 20 July 2008 when the OMI pixel size over Pullman was closest to nadir and the DS-MFDOAS $SO_2$ cloud sampling location was farthest from the pixel boundary. There were two OMI overpasses on 19 July 2008 with much larger spatial averaging (cross-track positions 11 and 60). In addition, the sampling location was close to the intersection of 4 pixels containing $SO_2$ VCDs ranging from ~1 to 0.2 DU.

[36] Table 2 shows OMI overpass data (operational LF data publicly available from NASA's Mirador search engine [http://mirador.gsfc.nasa.gov/cgibin/mirador/collectionlist.pl?keyword = omso2] and off-line ISF retrievals) for the MFDOAS location during the Okmok $SO_2$ cloud transit from 18–20 July. The best agreement occurred on July 19 at 20:29 UT (Table 2 and Figures 2 and 8) when OMI LF (OMSO2) and MFDOAS $SO_2$ VCDs differ by only ~0.07 DU (2%), well within the uncertainty of both data sets (~0.2–0.3 DU). This agreement is achieved without accounting for any spatial variability of $SO_2$ within the area covered by the OMI footprint (42 × 13 $km^2$), which might be expected to induce differences between the spatially averaged OMI measurements and the 1° FOV of the MFDOAS. This could indicate a lack of significant spatial variability in the volcanic cloud at the time of the measurements. The OMI overpass at 22:07 UT on 19 July also measured $SO_2$ over Pullman at the eastern edge of the OMI orbit (cross-track pixel 60; Figure 8). Despite the much larger OMI FOV at this extreme look angle, the agreement between the OMI and MFDOAS $SO_2$ VCD was still good. The difference between MFDOAS $SO_2$ VCD and OMSO2 and ISF were 0.4 DU (23%) and 0.26 DU (15%), respectively (Table 2). Comparison of OMI data with the coincident MFDOAS measurements at 21:12 on 20 July (1.22 DU) also resulted in good agreement (within error) between the two data sets (OMSO2: 0.18 DU ≈ 15% and ISF: −0.2DU ≈ −16%). Correlation between OMI LF/ISF and DS-MFDOAS $SO_2$ vertical columns for the three OMI overpasses is shown in Figure 9.

## 5. Conclusions

[37] In this study OMI operational (LF) and off line (ISF) $SO_2$ column retrievals were compared to direct Sun ground-based MFDOAS measurements over Pullman, WA during the Okmok volcanic $SO_2$ cloud transit on 18–20 July 2008. This comparison demonstrates that the operational OMI $SO_2$ retrievals provide accurate results for low $SO_2$ VCDs in the UTLS under cloud-free conditions and represents the first robust validation of the OMI $SO_2$ measurements. Furthermore, the agreement between retrievals based on down-looking (OMI) and up-looking (MFDOAS) measurements indicates that the operational OMI $SO_2$ algorithm accurately accounts for UV reflection and scattering beneath the volcanic cloud. Data validation is a necessary exercise during any satellite mission, and our results provide confidence in the long-term volcanic $SO_2$ emissions inventory derived from OMI and in the use of the OMI $SO_2$ measurements for climate modeling.

[38] Validation of higher $SO_2$ VCDs (100 DU or more) in fresh volcanic eruption clouds and of lower tropospheric

$SO_2$ VCDs in quiescent volcanic plumes is also needed. Such measurements are more challenging than the Okmok volcanic cloud validation documented here, requiring ground-based or aircraft measurements in close proximity to active volcanic vents, where $SO_2$ column amounts are highest (e.g., S. A. Carn et al., In-situ measurements of tropospheric volcanic plumes in Ecuador and Colombia during TC[4], submitted to *Journal of Geophysical Research*, 2010). More opportunities are arising as global networks such as NOVAC are implemented [*Galle et al.*, 2009], deploying quality instruments near to degassing volcanoes and providing more sophisticated radiative transfer analyses.

[39] **Acknowledgments.** The Dutch-Finnish built OMI instrument is part of the NASA EOS Aura satellite payload. The OMI project is managed by NIVR and KNMI in Netherlands. The authors would like to thank the KNMI OMI team for producing L1B radiance data and the U. S. OMI operational team for $SO_2$ analysis and continuing support. Nickolay Krotkov, Arlin Krueger, and Simon Carn acknowledge NASA funding of OMI $SO_2$ research and validation (grants NNG06GI00G and NNG06GJ02G); Arlin Krueger, Simon Carn, and Kai Yang also acknowledge NASA CAN (NNS06AA05G) funding. The WSU instrument and field activities were supported by grant NNG05GR56G from NASA to Washington State University. The MFDOAS instrument was built in the WSU instrument shop by Kurt Hutchinson and Gary Held.

## References

Aliwell, S. R., et al. (2002), Analysis for BrO in zenith-sky spectra: An intercomparison exercise for analysis improvement, *J. Geophys. Res.*, *107*(D14), 4199, doi:10.1029/2001JD000329

Andres, R. (2001), The effects of volcanic ash on COSPEC measurements, *J. Volcanol. Geotherm. Res.*, *108*(1–4), 237–244, doi:10.1016/S0377-0273(00)00288-2.

Benkovitz, C. M., S. E. Schwartz, M. P. Jensen, M. A. Miller, R. C. Easter, and T. S. Bates (2004), Modeling atmospheric sulfur over the Northern Hemisphere during the Aerosol Characterization Experiment 2 experimental period, *J. Geophys. Res.*, *109*, D22207, doi:10.1029/2004JD004939.

Berglen, T. F., G. Myhre, I. S. Isaksen, V. Vestreng, and S. J. Smith (2007), Sulphate trends in Europe: Are we able to model the recent observed decrease?, *Tellus, Ser B*, *59*(4), 773–786, doi:10.1111/j.1600-0889.2007.00289.x.

Bernhard, G., R. D. Evans, G. J. Labow, and S. J. Oltmans (2005), Bias in Dobson total ozone measurements at high latitudes due to approximations in calculations of ozone absorption coefficients and air mass, *J. Geophys. Res.*, *110*, D10305, doi:10.1029/2004JD005559.

Berresheim, H., P. Wine, and D. Davis (1995), Sulfur in the Atmosphere, in *Composition Chemistry, and Climate of the Atmosphere*, edited by H. B. Singh, p. 544, Wiley.

Bhartia, P. K., and C. W. Wellemeyer (2004), Version 8 TOMS Algorithm Theoretical Basis Document. (Available at http://toms.gsfc.nasa.gov/version8/version8_update.html)

Bluth, G. J. S., C. C. Schnetzler, A. J. Krueger, and L. S. Walter (1993), The contribution of explosive volcanism to global atmospheric sulphur dioxide concentrations, *Nature*, *366*, 327–329.

Bobrowski, N., and U. Platt (2007), $SO_2$/BrO ratios studied in five volcanic plumes, *J. Volcanol. Geotherm. Res.*, *166*(3–4), 147–160.

Bogumil, K., et al. (2003), Measurements of molecular absorption spectra with the SCIAMACHY preflight model: Instrument characterization and reference data for atmospheric remote sensing in the 230-2380 nm region, *J. Photochem. Photobiol. A.*, *157*, 167–184.

Bovensmann, H., J. P. Burrows, M. Buchwitz, J. Frerick, S. Noël, V. V. Rozanov, K. V. Chance, and A. P. H. Goede (1999) SCIAMACHY: Mission objectives and measurement modes, *J. Atmos. Sci.*, *56*(2), 127–150.

Bramstedt, K., et al. (2004), SCIAMACHY $SO_2$ column validation (working title), *Proc. ENVISAT ACVE2 workshop, SP-562*, May 3–7.

Brasseur, G., and C. Granier (1992), Mount Pinatubo aerosols, chlorofluorocarbons, and ozone depletion, *Science*, *257*(5074), 1239–1242, doi:10.1126/science.257.5074.1239.

Burrows, et al. (1999), The Global Ozone Monitoring Experiment (GOME): Mission concept and first scientific results, *J. Atmos. Sci.*, *56*(2), 151–175.

Burton, M., T. Caltabiano, F. Murè, G. Salerno, and D. Randazzo (2009), $SO_2$ flux from Stromboli during the 2007 eruption: Results from the FLAME network and traverse measurements, *J. Volcanol. Geotherm. Res.*, *182*(3–4), 214–220, doi:10.1016/j.jvolgeores.2008.11.025.

Carn, S. A., A. J. Krueger, G. J. S. Bluth, S. J. Schaefer, N. A. Krotkov, I. M. Watson, and S. Datta (2003), Volcanic eruption detection by the Total Ozone Mapping Spectrometer (TOMS) instruments: A 22-year record of sulfur dioxide and ash emissions, in *Volcanic Degassing*, edited by C. Oppenheimer, D. M. Pyle and J. Barclay, Geol. Soc. London, Spec. Publ., *213*, 177–202.

Carn, S. A. (2004), Eruptive and passive degassing of sulfur dioxide at Nyiragongo volcano (D.R. Congo): The 17 January 2002 eruption and its aftermath, *Acta Vulcanol.*, *14–15*, 75–86.

Carn, S. A., N. A. Krotkov, A. J. Krueger, K. Yang, and P. F. Levelt (2007), Sulfur dioxide emissions from Peruvian copper smelters detected by the ozone monitoring instrument, *Geophys. Res. Lett.*, *34*, L09801, doi:10.1029/2006GL029020.

Carn, S. A., A. J. Krueger, N. A. Krotkov, S. Arellano, and K. Yang (2008a), Daily monitoring of Ecuadorian volcanic degassing from space, *J. Volcanol. Geotherm. Res.*, *176*(1), 141–150, doi:10.1016/j.jvolgeores.2008.01.029.

Carn, S. A., A. J. Krueger, N. A. Krotkov, K. Yang, and K. Evans (2008b), Tracking volcanic sulfur dioxide clouds for aviation hazard mitigation, *Nat. Hazards*, *51*(2), 325–343, doi:10.1007/s11069-008-9228-4.

Cede, A., J. Herman, A. Richter, N. Krotkov, and J. Burrows (2006), Measurements of nitrogen dioxide total column amounts using a Brewer double spectrophotometer in direct Sun mode, *J. Geophys. Res.*, *111*, D05304, doi:10.1029/2005JD006585.

Charlson, R. J., J. Langner, and H. Rodhe (1990), Sulphate aerosol and climate, *Nature*, *348*, 22.

Chen, J., J. Vaughan, J. Avise, S. O'Neill, and B. Lamb (2008), Enhancement and evaluation of the AIRPACT ozone and PM2.5 forecast system for the Pacific Northwest, *J. Geophys. Res.*, *113*, D14305, doi:10.1029/2007JD009554

Chin, M., R. B. Rood, S.-J. Lin, J.-F. Müller, and A. M. Thompson (2000), Atmospheric sulfur cycle simulated in the global model GOCART: Model description and global properties, *J. Geophys. Res.*, *105*(D20), 24,671–24,687.

Dickerson, R. R., et al. (2007), Aircraft observations of dust and pollutants over northeast China: Insight into the meteorological mechanisms of transport, *J. Geophys. Res.*, *112*, D24S90, doi:10.1029/2007JD008999.

Edmonds, M., R. Herd, B. Galle, and C. Oppenheimer (2003), Automated, high time-resolution measurements of $SO_2$ flux at Soufrière Hills Volcano, Montserrat, *Bull. Volcanol.*, *65*(8), 578–586, doi:10.1007/s00445-003-0286-x.

Eisinger, M., and J. Burrows (1998), Tropospheric sulfur dioxide observed by the ERS-2 GOME Instrument, *Geophys. Res. Lett.*, *25*(22), 4177–4180.

Fioletov, V. E., E. Griffioen, J. B. Kerr, D. I. Wardle, and O. Uchino (1998), Influence of volcanic sulfur dioxide on spectral UV irradiance as measured by Brewer spectrophotometers, *Geophys. Res. Lett.*, *25*(10), 1665–1668.

Fioletov, V. E., et al. (2008), Performance of the ground-based total ozone network assessed using satellite data, *J. Geophys. Res.*, *113*, D14313, doi:10.1029/2008JD009809.

Galle, B., C. Oppenheimer, A. Geyer, A. J. S. McGonigle, M. Edmonds, and L. Horrocks (2003), A miniaturised ultraviolet spectrometer for remote sensing of SO2 fluxes: A new tool for volcano surveillance, *J. Volcanol. Geotherm. Res.*, *119*(1–4), 241–254, doi:10.1016/S0377-0273(02)00356-6.

Galle, B., N. Bobrowski, S. Carn, J. Durieux, M. Johansson, M. Kasereka, C. Oppenheimer, M. Yalire, and Y. Zhang (2005), Gas emissions from Nyiragongo volcano D. R. of Congo, measured by UV mini-DOAS spectroscopy, *Geophys. Res. Abstr.*, *7*, 08332, EGU General Assembly, Vienna, Austria.

Galle, B., M. Johansson, C. Rivera, Y. Zhang, M. Kihlman, C. Kern, T. Lehmann, U. Platt, S. Arellano, and S. Hidalgo (2009), NOVAC – A global network for volcano gas monitoring: Network layout and instrument description, *J. Geophys. Res.*, *115*, D05304, doi:10.1029/2009JD011823.

Giannitrapani, M., A. Bowman, E. Scott, and R. Smith (2006), Sulphur dioxide in Europe: Statistical relationships between emissions and measured concentrations, *Atmos. Environ.*, *40*, 2524–2532.

Giannitrapani, M., A. Bowman, E. Scott, and R. Smith (2007), Temporal analysis of spatial covariance of SO2 in Europe from 1990 to 2001, *Environmetrics*, *1*, 1–12.

Graf, H.-F., J. Feichter, and B. Langmann (1997), Volcanic sulfur emissions: Estimates of source strength and its contribution to the global sulfate distribution, *J. Geophys. Res.*, *102*(D9), 10,727–10,738.

Halmer, M. M., H.-U. Schmincke, and H.-F. Graf (2002), The annual volcanic gas input into the atmosphere, in particular into the stratosphere: A global data set for the past 100 years, *J. Volcanol. Geotherm. Res.*, *115*, 511–528.

Herman, J., A. Cede, E. Spinei, G. Mount, M. Tzortziou, and N. Abuhassan (2009), $NO_2$ column amounts from ground-based Pandora and MFDOAS spectrometers using the direct Sun DOAS technique: Intercomparisons and application to OMI validation, *J. Geophys. Res.*, *114*, D13307, doi:10.1029/2009JD011848.

Hoff, R. M., and M. M. Millan (1981), Remote $SO_2$ mass flux measurements using COSPEC, *Air Pollut. Control Assoc. J.*, *31*, 381–384.

Hofmann, D. J., and S. Solomon (1989), Ozone destruction through heterogeneous chemistry following the eruption of El Chichón, *J. Geophys. Res.*, *94*(D4), 5029–5041.

Holland, D. M., O. V. De, L. H. Cox, and R. L. Smith (2000), Estimation of regional trends in sulfur dioxide over the eastern United States, *Environmetrics*, *1*(4), 373–393.

Horrocks, L. A., C. Oppenheimer, M. R. Burton, H. J. Duffell, N. M. Davies, N. A. Martin, and W. Bell (2001), Open-path Fourier transform infrared spectroscopy of $SO_2$: An empirical error budget analysis, with implications for volcano monitoring, *J. Geophys. Res.*, *106*(D21), 27,647–27,659, doi:10.1029/2001JD000343.

Hunt, W. H., D. M. Winker, M. A. Vaughan, K. A. Powell, P. L. Lucker, and C. Weimer (2009), CALIPSO lidar description and performance assessment, *J. Atmos. Oceanic Technol.*, *26*(7), 1214–1228.

Joiner, J., and A. Vasilkov (2006), First results from the OMI rotational Raman scattering cloud pressure algorithm, *IEEE Trans. Geosci. Remote Sensing*, *44*(5), 1272–1282, doi:10.1109/TGRS.2005.861385.

Justice, C. O., J. R. G. Townshend, E. F. Vermote, E. Masuoka, R. E. Wolfe, N. Saleous, D. P. Roy, and J. T. Morisette (2002), An overview of MODIS land data processing and product status, *Remote Sens. Environ.*, *83*(1–2), 3–15, doi:10.1016/S0034-4257(02)00084-6.

Kato, N., and H. Akimoto (2007), Anthropogenic emissions of $SO_2$ and $NO_x$ in Asia: Emission inventories, *Atmos. Environ.*, *41*, S171–S191.

Katsouyanni, K., et al. (1997), Short-term effects of ambient sulphur dioxide and particulate matter on mortality in 12 European cities: Results from time series data from the APHEA project. Air pollution and health: A European approach, *BMJ(Clinical Research Ed.)*, *314*(7095), 1658–1663.

Kern, C., H. Sihler, L. Vogel, C. Rivera, M. Herrera, and U. Platt (2008), Halogen oxide measurements at Masaya Volcano, Nicaragua using active long path differential optical absorption spectroscopy, *Bull. Volcanol.*, *71*(6), 659–670, doi:10.1007/s00445-008-0252-8.

Kern, C., T. Deutschmann, L. Vogel, M. Wöhrbach, T. Wagner, and U. Platt (2009), Radiative transfer corrections for accurate spectroscopic measurements of volcanic gas emissions, *Bull. Volcanol.*, *72*(2), 233–247, doi:10.1007/s00445-009-0313-7.

Kerr, J. B., and W. J. Evans (1987), Comparison of ground-based and TOMS measurements of $SO_2$ from volcanic emissions, in *Scientific and Operational Requirements for TOMS Data*, edited by A. J. Krueger, 60–69, *NASA Conf. Publ. 2497*, NASA, Washington, D. C. (http://ntrs.nasa.gov/archive/nasa/casi.ntrs.nasa.gov/19880004392_1988004392.pdf)

Kerr, J. B. (2002), New methodology for deriving total ozone and other atmospheric variables from Brewer spectrophotometer direct Sun spectra, *J. Geophys. Res.*, *107*(D23), 4731, doi:10.1029/2001JD001227.

Khokhar, M. F., et al. (2005), Satellite remote sensing of atmospheric $SO_2$: Volcanic eruptions and anthropogenic emissions, in *Proceedings of the 2004 Envisat & ERS Symposium* (CD ROM), ESA SP-572, edited by H. Lacoste and L. Ouwehand, Salzburg, Austria, 6–10 Sept.

Krotkov, N. A., S. A. Carn, A. J. Krueger, P. K. Bhartia, and K. Yang (2006), Band residual difference algorithm for retrieval of SO2 from the Aura ozone monitoring instrument (OMI), *IEEE Trans. Geosci. Remote Sens.*, *44*(5), 1259–1266, doi:10.1109/TGRS.2005.861932.

Krotkov, N. A., et al. (2008), Validation of $SO_2$ retrievals from the ozone monitoring instrument over NE China, *J. Geophys. Res.*, *113*, D16S40, doi:10.1029/2007JD008818.

Krueger, A. J. (1983), Sighting of El Chichon sulfur dioxide clouds with the Nimbus 7 total ozone mapping spectrometer, *Science*, *220*(4604), 1377–1379, doi:10.1126/science.220.4604.1377.

Krueger, A. J., S. J. Schaefer, N. Krotkov, G. Bluth, and S. Barker (2000), Ultraviolet remote sensing of volcanic emissions, in *Remote Sensing of Active Volcanism*, edited by P. J. Mouginis-Mark, J. A. Crisp, and J. H. Fink, *Geophys. Monogr.* 116, pp. 25–43, AGU, Washington, D. C.

Krueger, A. J., N. A. Krotkov, and S. A. Carn (2008), El Chichon: The genesis of volcanic sulfur dioxide monitoring from space, *J. Volcanol. Geotherm. Res.*, *175*, 408–414, doi:10.1016/j.jvolgeores.2008.02.026.

Larsen, J., C. Neal, P. Webley, J. Freymueller, M. Haney, S. McNutt, D. Schneider, S. Prejean, J. Schaefer, and R. Wessels (2009), Eruption of Alaska volcano breaks historic pattern, *EOS Trans. AGU*, *90*(20), 173–174.

Lee, C., A. Richter, M. Weber, and J. P. Burrows (2008), $SO_2$ Retrieval from SCIAMACHY using the Weighting Function DOAS (WFDOAS) technique: Comparison with Standard DOAS retrieval, *Atmos. Chem. Phys.*, *8*(20), 6137–6145.

Levelt, P. F., G. H. J. van den Oord, M. R. Dobber, A. Malkki, H. Visser, J. de Vries, P. Stammes, J. O. V. Lundell, and H. Saari (2006), The ozone monitoring instrument, *IEEE Trans. Geo. Rem. Sens.*, *44*, 1093–1101.

Likens, G. E., and F. H. Bormann (1974), Acid rain: A serious regional environmental problem, *Science*, *184*(4142), 1176–1179, doi:10.1126/science.184.4142.1176.

Louban, I., N. Bobrowski, D. Rouwet, S. Inguaggiato, and U. Platt (2009), Imaging DOAS for volcanological applications, *Bull. Volcanol.*, *71*(7), 753–765, doi:10.1007/s00445-008-0262-6.

Malicet, J., D. Daumont, J. Charbonnier, C. Parisse, A. Chakir, and J. Brion (1995), Ozone UV spectroscopy: II. Absorption cross-sections and temperature dependence, *J. Atmos. Chem.*, *21*, 263–273.

Miller, C. A., C. A. Werner, M. Edmonds, and R. A. Herd (2006), A remotely operated, automatic scanning DOAS system at White Island, New Zealand, *EOS Trans. AGU*, *87*(52), Fall Meet. Suppl., Abstract V53A-1722.

Moffat, A. J., and M. M. Millan (1971), The applications of optical correlation techniques to the remote sensing of SO2 plumes using sky light, *Atmos. Environ.*, *5*(8), 677–690, doi:10.1016/0004-6981(71)90125-9.

Neal, C. A., J. F. Larsen, and J. Schaefer (2009) The July–August 2008 hydrovolcanic eruption of Okmok Volcano, Umnak Island, *Alaska Geol. Soc. Newsl.*, *39*(5).

Noxon, J. F. (1975), Nitrogen dioxide in the stratosphere and troposphere measured by ground-based absorption spectroscopy, *Science*, *189*(4202), 547–549, doi:10.1126/science.189.4202.547.

Oppenheimer, C., P. Francis, M. Burton, A. Maciejewski, and L. Boardman (1998), Remote measurement of volcanic gases by Fourier transform infrared spectroscopy, *Appl. Phys. B*, *67*(4), 505–515, doi:10.1007/s003400050536.

Platnick, S., M. King, S. Ackerman, W. Menzel, B. Baum, J. Riedi, and R. Frey (2003), The MODIS cloud products: Algorithms and examples from terra, *IEEE Trans. Geosci. Remote Sens.*, *41*(2), 459–473, doi:10.1109/TGRS.2002.808301.

Platt, U. (1994), Differential Optical Absorption Spectroscopy (DOAS), in *Air Monitoring by Spectroscopic Techniques*, edited by M. W. Sigrist, John Wiley, New York.

Platt, U., and J. Stutz (2008), *Differential Optical Absorption Spectroscopy: Principles and Applications*, Springer, Berlin.

Richter, A., F. Wittrock, J. P. Burrows (2006), $SO_2$ Measurements with SCIAMACHY, March 2006 Atmospheric Science Conference, in *Proceedings of the conference held 8-12 May, 2006 at ESRIN, Frascati Italy* (CDROM), edited by H. Lacoste and L. Ouwehand, p.51.1, ESA SP-628, Euro. Space Agency.

Robock, A. (2000), Volcanic eruptions and climate, *Rev. Geophys.*, *38*(2), 191–219.

Rodríguez, L. A., I. M. Watson, M. Edmonds, G. Ryan, V. Hards, C. M. Oppenheimer, and G. J. Bluth (2008), $SO_2$ loss rates in the plume emitted by Soufrière Hills volcano, Montserrat, *J. Volcanol. Geotherm. Res.*, *173* (1–2), 135–147, doi:10.1016/j.jvolgeores.2008.01.003.

Rose, W. I., et al. (2006), Atmospheric chemistry of a 33–34 hour old volcanic cloud from Hekla volcano (Iceland): Insights from direct sampling and the application of chemical box modeling, *J. Geophys. Res.*, *111*, D20206, doi:10.1029/2005JD006872.

Salerno, G., M. Burton, C. Oppenheimer, T. Caltabiano, D. Randazzo, N. Bruno, and V. Longo (2009), Three-years of $SO_2$ flux measurements of Mt. Etna using an automated UV scanner array: Comparison with conventional traverses and uncertainties in flux retrieval, *J. Volcanol. Geotherm. Res.*, *183*(1–2), 76–83, doi:10.1016/j.jvolgeores.2009.02.013.

Seinfeld, J. H., and S. N. Pandis (1998), *Atmospheric Chemistry and Physics: From Air Pollution to Climate Change*, John Wiley, New York.

Schreiner, A. J., T. J. Schmit, and W. P. Menzel (2001), Observations and trends of clouds based on GOES sounder data, *J. Geophys. Res.*, *106*(D17), 20,349–20,363.

Sommer, T. (2008), Direct Sun light measurements of volcanic plumes using differential optical absorption spectroscopy, Diploma thesis, Univ. of Heidelberg, Germany.

Stern, D. (2005), Global sulfur emissions from 1850 to 2000, *Chemosphere*, *58*(2), 163–175, doi:10.1016/j.chemosphere.2004.08.022.

Ta, W., C. Wei, and F. Chen (2005), Long-term measurements of SO sub (2) dry deposition over Gansu Province, China, *Atmos. Environ.*, *39*(37), 7095–7105.

Textor, C., H.-F. Graf, M. Herzog, and J. M. Oberhuber (2003), Injection of gases into the stratosphere by explosive volcanic eruptions, *J. Geophys. Res.*, *108*(D19), 4606, doi:10.1029/2002JD002987.

Thomas, W., T. Erbertseder, T. Ruppert, M. van Roozendael, J. Verdebout, C. Meleti, D. Balis, and C. Zerefos (2005), On the retrieval of volcanic sulfur dioxide emissions from GOME backscatter measurements, *J. Atmos. Chem.*, *50*, 295–320, doi: 10.1007/s10874-005-5544-1

Thomason, L. W., and M. C. Pitts (2008), CALIPSO observations of volcanic aerosol in the stratosphere, *Proc. SPIE*, *7153*, 71530O, doi:10.1117/12.804090.

Thornton, D. C., A. R. Bandy, B. W. Blomquist, J. D. Bradshaw, and D. R. Blake (1997), Vertical transport of sulfur dioxide and dimethyl sulfide in deep convection and its role in new particle formation, *J. Geophys. Res.*, *102*(D23), 28,501–28,509.

Thornton, D. C., A. R. Bandy, B. W. Blomquist, A. R. Driedger, and T. P. Wade (1999), Sulfur dioxide distribution over the Pacific Ocean 1991–1996, *J. Geophys. Res.*, *104*(D5), 5845–5854.

Van Roozendael and Fayt (2001) WinDOAS 2.1 Software User Manual, Belgian Institute for Space Aeronomy (BIRA-IASB).

U. S. Environmental Protection Agency (2008), Latest Findings on National Air Quality: Status and trends through 2006, EPA-454/R-07-007, Office of Air Quality Planning and Standards Air Quality Assessment Division Research Triangle Park, North Carolina.

Vandaele, A. C., C. Hermans, P. C. Simon, M. Carleer, R. Colin, S. Fally, M. F. Mérienne, A. Jenouvrier, and B. Coquart (1998), Measurements of the $NO_2$ absorption cross-section from 42000 $cm^{-1}$ to 10000 $cm^{-1}$ (238-1000 nm) at 220 K and 294 K, *J.Q.S.R.T.*, *59*, 171–184.

von Glasow, R., N. Bobrowski, and C. Kern (2009), The effects of volcanic eruptions on atmospheric chemistry, *Chem. Geol.*, *263*(1–4), 131–142, doi:10.1016/j.chemgeo.2008.08.020.

Ware, J. H., B. G. Ferris Jr., D. W. Dockery, J. D. Spengler, D. O. Stram, F. E. Speizer (1986), Effects of ambient sulfur oxides and suspended particles on respiratory health of preadolescent children, *Am. Rev. Respir. Dis*, *5*, 834–842.

Wilmouth, D. M., T. F. Hanisco, N. M. Donahue, and J. G. Anderson (1999), Fourier transform ultraviolet spectroscopy of the A $^2\Pi_{3/2} \leftarrow$ X $^2\Pi_{3/2}$ transition of BrO, *J. Phys. Chem. A*, *103*, 8935–8945.

Yang, K., N. A. Krotkov, A. J. Krueger, S. A. Carn, P. K. Bhartia, and P. F. Levelt (2007), Retrieval of large volcanic $SO_2$ columns from the Aura ozone monitoring instrument: Comparison and limitations, *J. Geophys. Res.*, *112*, D24S43, doi:10.1029/2007JD008825.

Yang, K., N. A. Krotkov, A. J. Krueger, S. A. Carn, P. K. Bhartia, and P. F Levelt (2009), Improving retrieval of volcanic sulfur dioxide from backscattered UV satellite observations. *Geophys. Res. Lett.*, *36*, L03102, doi:10.1029/2008GL036036.

Yang, K., X. Liu, P. K. Bhartia, N. A. Krotkov, S. A. Carn, E. J. Hughes, A. J. Krueger, R. J. D. Spurr, and S. G. Trahan (2010), Direct retrieval of sulfur dioxide amount and altitude from spaceborne hyper-spectral UV measurements: Theory and application, *J. Geophys. Res.*, doi:10.1029/2010JD013982, in press.

S. A. Carn, Department of Geological and Mining Engineering and Sciences, Michigan Technological University, Houghton, MI 49931, USA. (scarn@mtu.edu)

N. A. Krotkov and K. Yang, Goddard Earth Sciences and Technology Center, University of Maryland Baltimore County, Baltimore, MD 21228, USA. (krotkov@chescat.gsfc.nasa.gov; Kai.Yang.1@gsfc.nasa.gov)

A. Krueger, Joint Center for Earth Systems Technology, University of Maryland Baltimore County, Baltimore, MD 21228, USA. (akrueger@umbc.edu)

G. H. Mount and E. Spinei, Laboratory for Atmospheric Research, Department of Civil and Environmental Engineering, Washington State University, Pullman, WA 99164-2910, USA. (espinei@wsu.edu; gmount@wsu.edu)